


Article

# Entropy Analysis of Carbon Nanotubes Based Nanofluid Flow Past a Vertical Cone with Thermal Radiation

Muhammad Ramzan <sup>1,2,\*</sup>, Mutaz Mohammad <sup>3,\*</sup> , Fares Howari <sup>4</sup> and Jae Dong Chung <sup>2</sup>

<sup>1</sup> Department of Computer Science, Bahria University, 44000 Islamabad, Pakistan

<sup>2</sup> Department of Mechanical Engineering, Sejong University, Seoul 143-747, Korea

<sup>3</sup> Department of Mathematics & Statistics, College of Natural and Health Sciences, Zayed University, 144543 Abu Dhabi, UAE

<sup>4</sup> College of Natural and Health Sciences, Zayed University, 144543 Abu Dhabi, UAE

\* Correspondence: mramzan@bahria.edu.pk (M.R.); mutaz.mohammad@zu.ac.ae (M.M.); Tel.: +92-300-51-22-700 (M.R.); +971-2-599-3496 (M.M.)

Received: 6 April 2019; Accepted: 14 May 2019; Published: 28 June 2019



**Abstract:** Our objective in the present study is to scrutinize the flow of aqueous based nanofluid comprising single and multi-walled carbon nanotubes (CNTs) past a vertical cone encapsulated in a permeable medium with solutal stratification. Moreover, the novelty of the problem is raised by the inclusion of the gyrotactic microorganisms effect combined with entropy generation, chemical reaction, and thermal radiation. The coupled differential equations are attained from the partial differential equations with the help of the similarity transformation technique. The set of conservation equations supported by the associated boundary conditions are solved numerically with the `bvp4c` MATLAB function. The influence of numerous parameters on the allied distributions is scrutinized, and the fallouts are portrayed graphically in the analysis. The physical quantities of interest including the skin friction coefficient and the rate of heat and mass transfers are evaluated versus essential parameters, and their outcomes are demonstrated in tabulated form. For both types of CNTs, it is witnessed that the velocity of the fluid is decreased for larger values of the magnetic and suction parameters. Moreover, the value of the skin friction coefficient drops versus the augmented bioconvection Rayleigh number. To corroborate the authenticity of the presented model, the obtained results (under some constraints) are compared with an already published paper, and excellent harmony is achieved in this regard.

**Keywords:** nanofluid; carbon nanotubes (SWCNTs and MWCNTs); solutal stratification; bioconvection; entropy generation

## 1. Introduction

Nanofluid, characterized by copious attractive features, including outstanding chemical and mechanical steadiness, significant improvement in thermal conductivity, etc. [1], is found to serve in a number of engineering applications, for example fuel-cells [2], porous materials [3], petroleum engineering [4], and biotechnology [5,6], among others. The pioneering work was done by Choi and Eastman [7] who found that thermal conductivity of the base fluid will increase from the insertion of metallic particles. This was followed by a study by Buongiorno [8] who studied the features of Brownian motion and thermophoresis in nanofluids. Later, Makinde and Aziz [9] deliberated on the flow of Newtonian fluid past a convectively heated surface. The flow of 3D couple stress nanofluid past an exponentially stretching surface associated with zero mass flux at the surface and convective boundary conditions was deliberated by Ramzan et al. [10]. Farooq et al. [11] examined Newtonian fluid

flow analytically over an exponentially stretching sheet under the influence of magneto hydrodynamics using the optimal homotopy analysis method. The nanofluid flows containing carbon nanotubes (CNTs) over a cone and an inclined permeable plate were studied numerically by Reddy et al. [12,13]. Sreedevi et al. [14] found a numerical solution for CNTs amalgamated nanofluid flow past a vertical cone with a convective boundary condition. The aqueous-silver non-Darcy Poiseuille nanofluid flow with entropy generation past a permeable media was studied by Shehzad et al. [15]. A few recent investigations highlighting nanofluid flows may be found in References [16–18].

CNTs are the hexagonal structure of carbon atoms that are rolled in a cylindrical shape. Carbon nanotubes possess unique features like corrosion resistance, high thermal conductivity, and exceptional strength [19]. Owing to these remarkable characteristics, CNTs are useful in numerous applications like nanotubes transistors, microwave amplifier, solar cells, chemical sensors, optics, drug delivery, prostheses, pharmacogenomics, and many other fields of engineering and material science [20–22]. Carbon nanotubes are labeled as multi-walled carbon nanotubes (MWCNTs) and single-walled carbon nanotubes (SWCNTs). Iijima [23] discovered carbon nanotubes in 1991. He first investigated MWCNTs utilizing the Krastschmer and Huffman method. This was followed by another exploration in 1993 by Bethune [24] who introduced the concept of SWCNTs. SWCNTs are comprised of carbon nanotubes with a diameter of 1 nm whereas MWCNTs is a collection of 2–50 carbon nanotubes with 0.34 nm spacing. Abundant studies may be found in the literature to highlight different aspects of CNTs. Ramasubramaniam et al. [25] found that single-walled CNTs are helpful in improving electrical conductivity. The idea of improved thermal conductivity using composite nanotubes was introduced by Xue [26]. Muhammad et al. [27] inspected the rotating flow of carbon nanotubes under the influence of heat generation/absorption and nonlinear thermal radiation past a linearly stretching surface. The flow of 3D viscous nanofluid containing CNTs with quartic chemical reaction and entropy generation analysis is expressed numerically by Kumar et al. [28]. The aqueous based nanofluid Darcy-Forchheimer 3D flow comprising CNTs past a permeable surface was examined analytically by Muhammad et al. [29]. The flow problem in Reference [29] is extended to homogeneous-heterogeneous reactions associated with convective boundary conditions is discussed by Alshomrani and Ullah [30]. Recent explorations studying CNTs nanofluid flow may be found in References [31–33] and those contained therein.

The aforementioned literature review reveals that abundant articles are available addressing the topic of nanofluid. But this subject gets narrower once we talk about nanofluid flow over a cone with nanotubes inserted into it. Furthermore, this exploration becomes unique when the above-mentioned characteristics are supported by entropy generation and gyrotactic microorganisms (see Table 1). The numerical solution of the problem is acquired with requisite discussion of plotted illustrations of involved parameters versus associated distributions.

**Table 1.** The studies on nanoliquid flow comprising carbon nanotubes (CNTs).

Authors	CNTs SWCNTs/MWCNTs	Entropy Generation	Gyrotactic Microorganisms	Flow over a Cone
Reddy et al. [12]	√	×	×	√
Reddy et al. [13]	√	×	×	×
Sreedevi et al. [14]	√	×	×	√
Kumar et al. [28]	√	√	×	×
Muhammad et al. [29]	√	×	×	×
Alshomrani & Ullah [30]	√	×	×	×
Lu et al. [31]	√	×	×	×
Ramzan et al. [32]	√	√	×	×
Lu et al. [33]	√	√	×	×
Present	√	√	√	√

(√) means effect is present, and (×) means effect is absent.

## 2. Mathematical Modeling

Let us assume a 2D aqueous fluid flow amalgamated with carbon nanotubes past a vertical cone in an absorbent media. The analysis is accompanied by solutal stratification, chemical reaction, and entropy generation (see Figure 1).

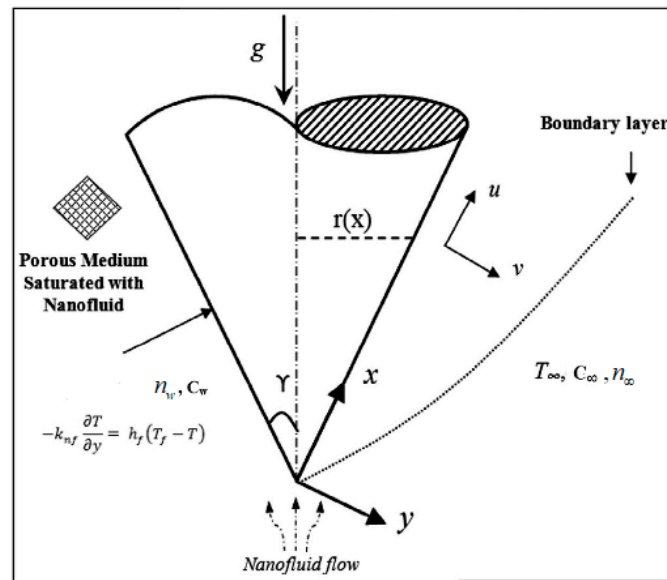


Figure 1. Physical model of the problem.

The flow of the fluid is along the  $x$ -axis past the cone surface. Along the  $y$ -axis, a magnetic field with strength  $B_0$  is enforced. The fluid is an aqueous based nanofluid containing both types of CNTs, whose thermo-physical characteristics are defined in Table 2. The governing system of equations representing the presented model are as follows [14]:

$$\frac{\partial(ru)}{\partial x} + \frac{\partial(rv)}{\partial y} = 0, \tag{1}$$

$$u \frac{\partial u}{\partial x} + v \frac{\partial u}{\partial y} = \frac{\mu_{nf}}{\rho_{nf}} \frac{\partial^2 u}{\partial y^2} - \frac{\mu_{nf}}{\rho_{nf}} \frac{1}{K} u + g[\beta(T - T_\infty) - \beta^*(C - C_\infty) - \beta^* \gamma(n - n_\infty) \Delta \rho] \cos \gamma - \frac{\sigma B_0^2}{\rho_{nf}} u, \tag{2}$$

$$u \frac{\partial T}{\partial x} + v \frac{\partial T}{\partial y} = \alpha_{nf} \frac{\partial^2 T}{\partial y^2} - \frac{1}{(\rho c_p)_{nf}} \frac{\partial q_r}{\partial y}, \tag{3}$$

$$u \frac{\partial C}{\partial x} + v \frac{\partial C}{\partial y} = D_m \frac{\partial^2 C}{\partial y^2} - K_r(C - C_\infty), \tag{4}$$

$$u \frac{\partial n}{\partial x} + v \frac{\partial n}{\partial y} + \frac{bW_c}{C_w - C_0} \frac{\partial}{\partial y} \left( n \frac{\partial C}{\partial y} \right) = D_n \frac{\partial^2 n}{\partial y^2}, \tag{5}$$

with the corresponding boundary conditions

$$v = V_1, u = 0, -k_{nf} \frac{\partial T}{\partial y} = h_f(T_f - T), C = C_w = C_0 + dx, n = n_w, \text{ at } y = 0, \tag{6}$$

$$u \rightarrow 0, T \rightarrow T_\infty, C \rightarrow C_\infty = C_0 + ex, n \rightarrow n_\infty, \text{ as } y \rightarrow \infty.$$

**Table 2.** Values of physical features of nanoparticles and water [14].

Physical Attributes	Liquid	Nanoparticles	
	H <sub>2</sub> O	SWCNTs	MWCNTs
C <sub>p</sub> (J/kg K)	4179	425	796
ρ (kg/m <sup>3</sup> )	997	2600	1600
k (W/mK)	0.613	6600	3000

Multi-walled carbon nanotubes (MWCNTs) and single-walled carbon nanotubes (SWCNTs).

The hypothetical relations are characterized as follows:

$$\mu_{nf} = \frac{\mu_f}{(1-\phi)^{2.5}}, \quad \nu_{nf} = \frac{\mu_{nf}}{\rho_{nf}}, \quad (7)$$

$$\rho_{nf} = (1-\phi)\rho_f + \phi\rho_{CNT}, \quad \alpha_{nf} = \frac{k_{nf}}{\rho_{nf}(c_p)_{nf}}, \quad (8)$$

$$\frac{k_{nf}}{k_f} = \frac{(1-\phi) + 2\phi \frac{k_{CNT}}{k_{CNT}-k_f} \ln\left(\frac{k_{CNT}+k_f}{2k_f}\right)}{(1-\phi) + 2\phi \frac{k_f}{k_{CNT}-k_f} \ln\left(\frac{k_{CNT}+k_f}{2k_f}\right)}. \quad (9)$$

Using the similarity transformations

$$\eta = \frac{y}{x}Ra_x^{1/4}, \quad \Psi = \alpha Ra_x^{1/4} f(\eta), \quad \theta(\eta) = \frac{T-T_\infty}{T_w-T_\infty}, \quad (10)$$

$$g(\eta) = \frac{C-C_\infty}{C_w-C_0}, \quad h(\eta) = \frac{n-n_\infty}{n_w-n_\infty},$$

Equation (1) is impartially fulfilled and Equations (2) to (6) obtain

$$f'''' + \frac{1}{Pr}(1-\phi)^{2.50}(1-\phi + \phi \frac{\rho_{CNT}}{\rho_f})\{3ff'' - \frac{1}{2}f'^2\} - k_1f' - (1-\phi)^{2.5}Mf' + (1-\phi)^{2.50}(1-\phi + \phi \frac{\rho_{CNT}}{\rho_f})[\theta - N_r g - R_b h] = 0, \quad (11)$$

$$\frac{k_{nf}}{k_f}(1 + R_d)\theta'' + \frac{3}{4}\left[1 - \phi + \phi \frac{(\rho C_p)_{CNT}}{(\rho C_p)_f}\right]f\theta' = 0, \quad (12)$$

$$g'' + \frac{3}{4}S_c f g' - S_c n f' - C_r g = 0, \quad (13)$$

$$h'' + \frac{3}{4}L_b f h' - P_e(h'g' + (h + \delta)g'') = 0, \quad (14)$$

and the boundary conditions (6) take the form

$$f(0) = V_0, \quad f'(0) = 0, \quad \frac{k_{nf}}{k_f}\theta'(0) = -B_1(1 - \theta(0)), \quad g(0) = 1 - n, \quad h(0) = 1, \quad (15)$$

$$f'(\infty) \rightarrow 0, \quad \theta(\infty) \rightarrow 0, \quad g(\infty) \rightarrow 0, \quad h(\infty) \rightarrow 0.$$

In the aforementioned equations, the dimensionless parameters are given by:

$$Pr = \frac{\nu_f}{\alpha}, \quad k_1 = \frac{x^2}{KRax^{1/2}}, \quad M = \frac{\sigma B_0^2 x^2}{\mu_f Ra_x^{1/2}}, \quad S_c = \frac{\alpha}{D_m}, \quad n = \frac{e}{d},$$

$$L_b = \frac{\alpha}{D_n}, \quad R_d = \frac{16T_\infty^3 \sigma^*}{3k^* k_{nf}}, \quad N_r = \frac{\beta^*(C_w - C_0)}{\beta(T_f - T_\infty)}, \quad R_b = \frac{\beta^* \gamma \Delta \rho \Delta n_w}{\beta(T_f - T_\infty)}, \quad (16)$$

$$C_r = \frac{K_r x^2}{D_m Ra_x^{1/2}}, \quad B_1 = \frac{h_f x}{Ra_x^{1/4} k_f}, \quad P_e = \frac{b W_c}{D_n}, \quad \delta = \frac{n_\infty}{n_w - n_\infty}.$$

The physically essential quantities, i.e., the skin friction, rate of heat and mass transfers, and local density of motile microorganisms, are appended below:

$$C_f = \frac{\tau_w}{\rho U_\infty^2}, Nu_x = \frac{xq_w}{k_f(T_w - T_\infty)}, Sh_x = \frac{xq_m}{D_m(C_w - C_0)}, Nn_x = \frac{xq_n}{D_n(n_w - n_\infty)}. \tag{17}$$

The aforementioned physical quantities in dimensionless form are appraised as follows:

$$\begin{aligned} C_f Ra_x^{1/4} &= \frac{1}{(1-\phi)^{2.5}} f''(0), \\ Nu_x Ra_x^{-1/4} &= -\frac{k_{nf}}{k_f} (1 + R_d) \theta'(0), \\ Sh_x Ra_x^{-1/4} &= -g'(0), \\ Nn_x Ra_x^{-1/4} &= -h'(0). \end{aligned} \tag{18}$$

Table 3 depicts a comparison with Khan et al. [34] for varied estimates of  $\phi$  in limiting case. An outstanding matching in both results is achieved. This reflects the corroboration of the presented outcomes.

**Table 3.** Evaluation of the presented model with Khan et al. [34] in limiting case.

$\phi$	$f'(0)$				$-\theta'(0)$			
	Khan et al. [34]		Existing Results		Khan et al. [34]		Existing Results	
	SWCNT	MWCNT	SWCNT	MWCNT	SWCNT	MWCNT	SWCNT	MWCNT
0.01	0.33894	0.33727	0.338910	0.337270	1.10553	1.07905	1.105710	1.079040
0.1	0.40811	0.39008	0.408120	0.390070	4.80627	4.27718	4.806290	4.277160
0.2	0.50452	0.46466	0.504530	0.464660	12.30317	10.56783	12.30352	10.56796

### Entropy Generation

The entropy generation of the presented model is specified as follows:

$$\begin{aligned} S_{gen}''' &= \underbrace{\frac{k_{nf}}{T_\infty^2} \left[ 1 + \frac{16T_\infty^3 \sigma^*}{3k^* k_{nf}} \right] \left( \frac{\partial T}{\partial y} \right)^2}_{HFI} + \underbrace{\frac{\mu_{nf}}{T_\infty} \left( \frac{\partial u}{\partial y} \right)^2 + \frac{\sigma}{T_\infty} B_0^2 u^2 + \frac{\mu_{nf}}{T_\infty K} u^2}_{FFI} \\ &\quad + \underbrace{\frac{RD}{C_\infty} \left( \frac{\partial C}{\partial y} \right)^2 + \frac{RD}{T_\infty} \left( \frac{\partial T}{\partial y} \right) \left( \frac{\partial C}{\partial y} \right)}_{Diffusive irreversibility}. \end{aligned} \tag{19}$$

In Equation (19), entropy is comprised of three terms, namely (i) HFI (heat transfer irreversibility), (ii) FFI (fluid friction irreversibility), and (iii) diffusion irreversibility. The entropy generation  $N_G$  is defined as:

$$N_G = \frac{S'''_{gen}}{S_0''''}, \tag{20}$$

where  $S'''_{gen}$  and  $S_0''''$  characterize the entropy generation rate and characteristic entropy generation rate, respectively, such that

$$\begin{aligned} N_G &= \frac{k_{nf}}{k_f} (1 + R) Ra_x \theta'^2 + \frac{1}{(1-\phi)^{2.5}} \frac{Br Ra_x}{\alpha} (f''^2 + k_1 f'^2) + \frac{Ra_x Br M}{\alpha} f'^2 \\ &\quad + \lambda \left( \frac{\zeta}{\alpha} \right)^2 Ra_x g'^2 + \frac{\zeta}{\alpha} Ra_x \lambda \theta' g'. \end{aligned} \tag{21}$$

Parameter used in above equation are define as,

$$\alpha = \frac{\Delta T}{T_\infty}, Br = \frac{\mu_f u_w}{k_f \Delta T}, \zeta = \frac{\Delta C}{C_\infty}, \lambda = \frac{RDC_\infty}{k_f}. \quad (22)$$

### 3. Results and Discussion

This section is devoted to comprehend the discussion of the graphical illustrations. The impressions of the miscellaneous parameters on entangled profiles are given in Figures 2–14. The numerical values of the parameters used are taken to be fixed as:  $\phi = 0.01$ ,  $N_r = P_e = k_1 = 0.5 = L_b$ ,  $S_c = B_1 = 1.0 = M = V_0$ ,  $R_b = n = R_d = 0.1 = C_r = \delta$  and  $Pr = 6.2$  unless otherwise stated. The ranges of parameters defined in the figures are  $0.4 \leq M \leq 1.0$ ,  $0.1 \leq k_1 \leq 0.7$ ,  $0.2 \leq N_r \leq 0.4$ ,  $0.1 \leq R_b \leq 0.3$ ,  $0.01 \leq \phi \leq 0.03$ ,  $0.5 \leq B_1 \leq 1.5$ ,  $0.1 \leq R_d \leq 0.7$ ,  $0.5 \leq S_c \leq 1.5$ ,  $0.1 \leq n \leq 0.5$ ,  $0.5 \leq P_e \leq 0.9$ ,  $0.5 \leq L_b \leq 0.7$ ,  $0.1 \leq \alpha \leq 0.3$ , and  $0.1 \leq \lambda \leq 0.5$ .

#### 3.1. Velocity Profile

The trend of axial velocity versus different parameters' effects is described in Figures 2–5. Figure 2 depicts the impact of the magnetic parameter  $M$  on the velocity field. The velocity of the fluid diminishes for increasing values of  $M$ . This is because of the strong Lorentz force that presents resistance to the fluid's movement that eventually lowers the fluid's movement. In Figure 3, the consequence of porous parameter  $k_1$  on the velocity profile is sketched. It is understood that the velocity is a decreasing function of  $k_1$ . Physically, more resistance against the fluid's movement is witnessed due to the augmented thickness of the permeable medium that results in feeble fluid velocity. The impact of the buoyancy ratio parameter  $N_r$  and the bioconvection Rayleigh number  $R_b$  on the velocity profile for both CNTs is depicted in Figures 4 and 5, respectively. It is witnessed that the velocity profile declines with increasing values of  $N_r$  and  $R_b$ . Higher values of the buoyancy ratio parameter mean an increase in the number of CNTs immersed into the aqueous solution, which increases the viscosity of the fluid and results in a decrease in fluid's velocity. Similarly, the velocity of the fluid is affected by the growth in the bioconvection Rayleigh number. This is due to the inertia force of the fluid motion being surpassed by the bioconvection. There is a decrease in speed of roughly 15.48% with an approximate increase in  $R_b$  of 400% [35].

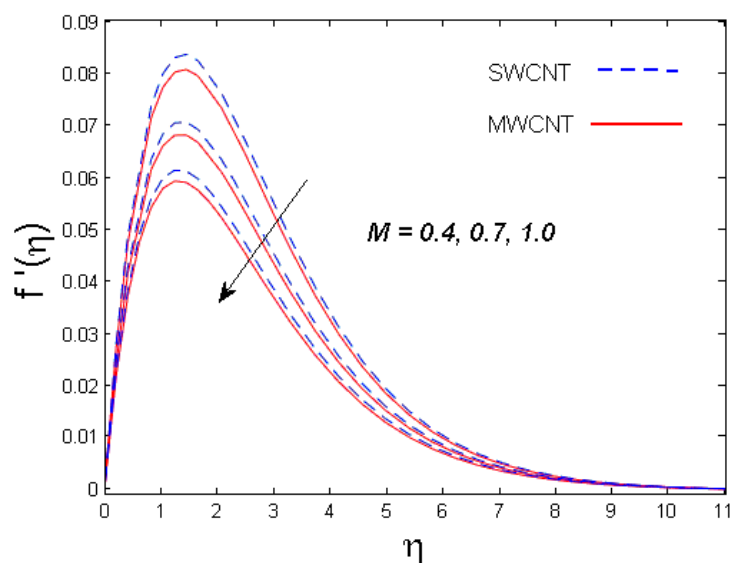


Figure 2. Consequence of  $M$  on  $f'(\eta)$ .

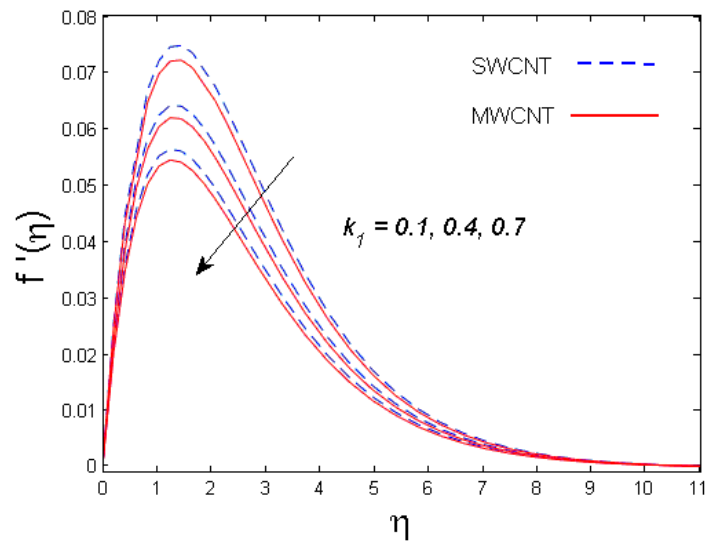


Figure 3. Consequence of  $k_1$  on  $f'(\eta)$ .

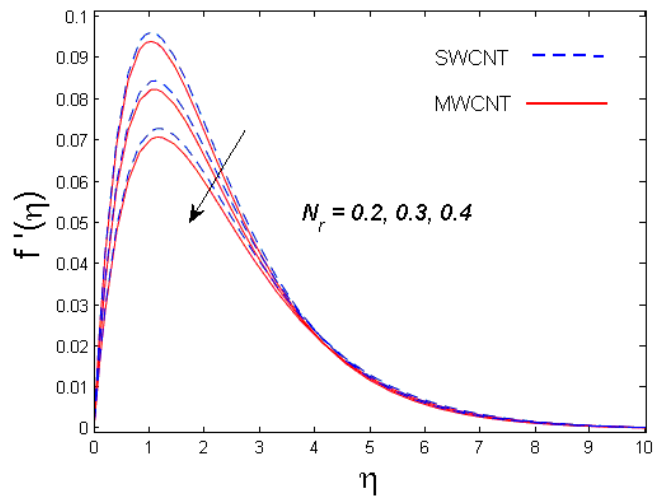


Figure 4. Consequence of  $N_r$  on  $f'(\eta)$ .

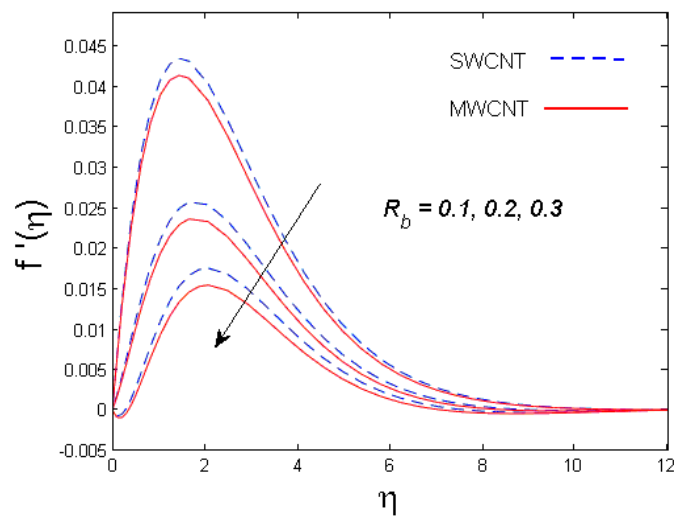


Figure 5. Consequence of  $R_b$  on  $f'(\eta)$ .

### 3.2. Temperature Profile

The outcome of solid volume fraction  $\phi$  on the temperature field is evident in Figure 6. The temperature profile is enhanced with increasing estimates of the solid volume fraction of the nanoparticles. It is also understood that the thermal boundary layer thickness is enhanced by augmenting the estimation of the solid volume fraction  $\phi$  for both nanotubes. This is all because of the enhancement in thermal conductivity of CNTs with solid volume fraction that becomes the main cause for augmented temperature. The effect of Biot number  $B_1$  is studied in Figure 7. It is perceived that with an upsurge in  $B_1$ , temperature distribution escalates for both SWCNT and MWCNT. Physically, larger estimates of  $B_1$  means more thermal resistance inside the cone in comparison to the boundary layer; consequently, a higher temperature of the fluid in the boundary layer area is witnessed. Figure 8 shows the influence of radiation parameter  $R_d$  on temperature profile. It was determined that larger values of  $R_d$  result in more energy being produced, which eventually raises the temperature of the fluid.

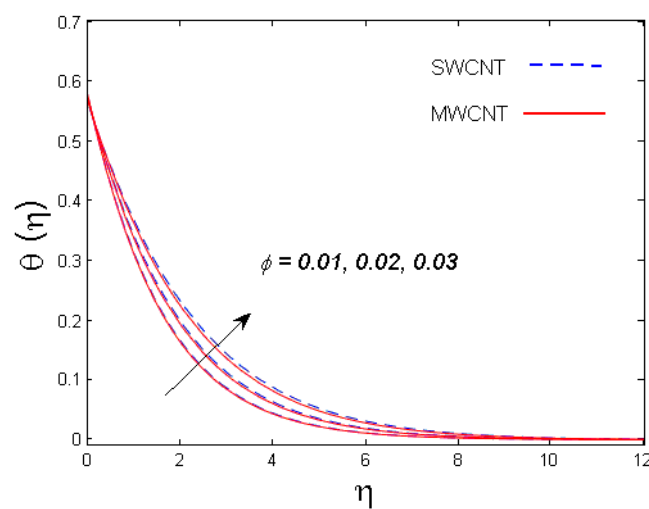


Figure 6. Consequence of  $\phi$  on  $\theta(\eta)$ .

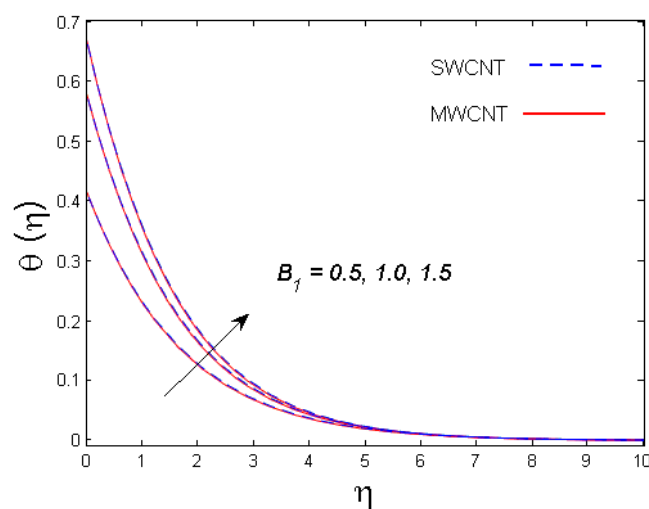


Figure 7. Consequence of  $B_1$  on  $\theta(\eta)$ .



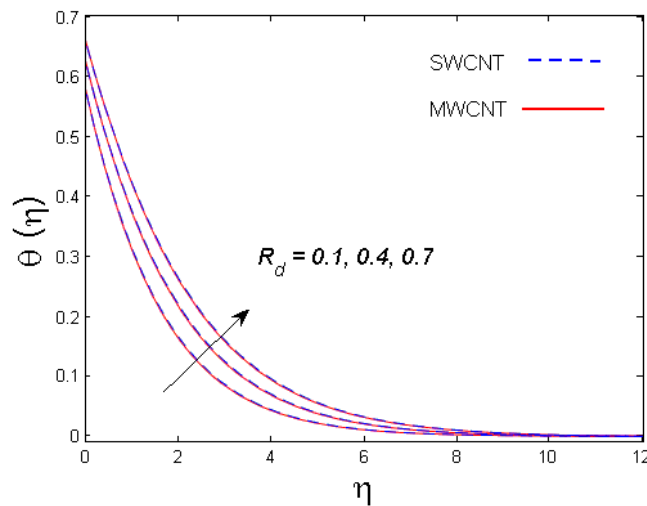


Figure 8. Consequence of  $R_d$  on  $\theta(\eta)$ .

### 3.3. Concentration Profile

The impact of numerous parameters on the concentration field is presented in Figures 9 and 10. Figure 9 depicts the influence of Schmidt number  $S_c$  on concentration distribution for both nanotubes. It is understood from the figure that the concentration field is a diminishing function of  $S_c$ . Since the Schmidt number is the proportion of kinematic viscosity and the molecular diffusion coefficient, higher values of  $S_c$  leads to a reduced molecular diffusion that ultimately lowers the concentration of the fluid. In Figure 10, the graph of concentration profile versus the solutal stratification  $n$  is depicted. It is clear that for improved values of  $n$ , the concentration of the fluid is diminished for both SWCNT and MWCNT nanotubes. In actuality, the lowering of concentration field is due of the concentration differences between the ambient fluid and the surface of the cone.

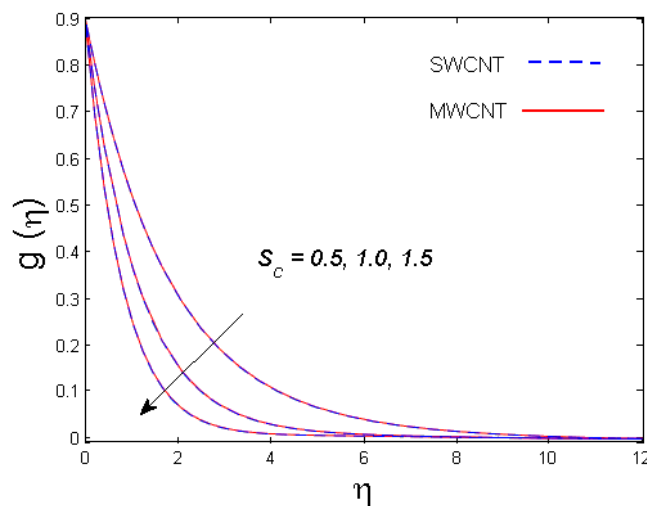


Figure 9. Consequence of  $S_c$  on  $g(\eta)$ .

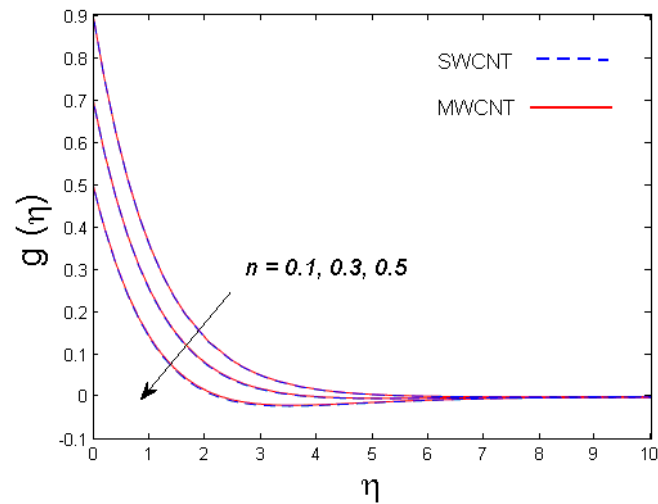


Figure 10. Consequence of  $n$  on  $g(\eta)$ .

### 3.4. Density of Motile Microorganism Profile

Figures 11 and 12 demonstrate the impacts of the bioconvection Péclet number and the bioconvection Lewis number on the density of motile microorganisms, respectively. It is observed that motile microorganisms decrease for both bioconvection Péclet number and bioconvection Lewis numbers. Indeed, higher estimates of the bioconvection Péclet and bioconvection Lewis numbers result in a decline in the microorganism diffusion, which ultimately results in the decay of the density and boundary layer thickness of motile microorganisms.

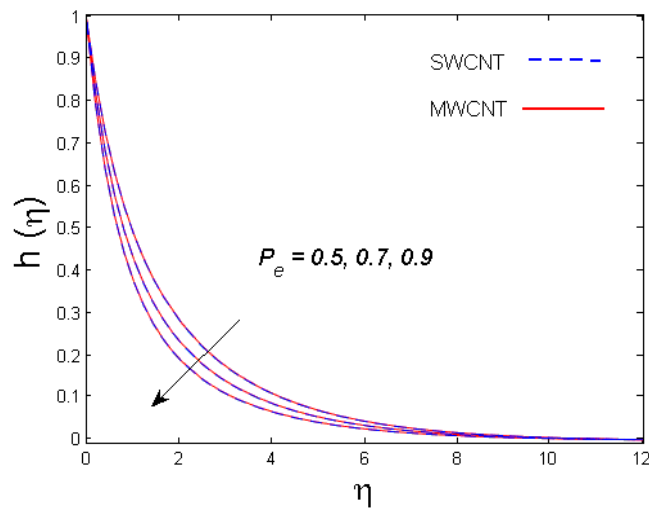


Figure 11. Consequence of  $P_e$  on  $h(\eta)$ .

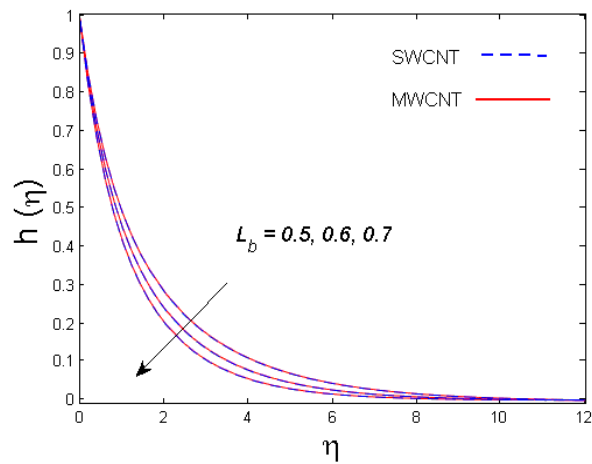


Figure 12. Consequence of  $L_b$  on  $h(\eta)$ .

### 3.5. Entropy Generation

From Figure 13, it is seen that increasing the temperature difference parameter  $\alpha$  decreases the entropy generation number  $N_G$  for both nanoparticles. Similarly, the local entropy generation increases for growing estimates of the diffusive constant parameter  $\lambda$  for both SWCNT and MWCNT, which is displayed in Figure 14.

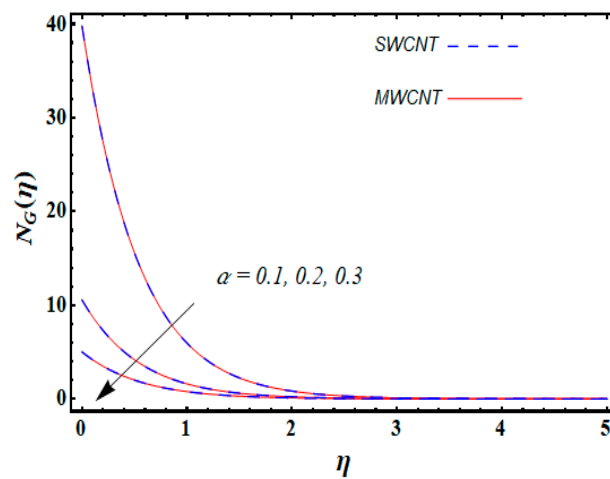


Figure 13. Consequence of  $\alpha$  on  $N_G(\eta)$ .

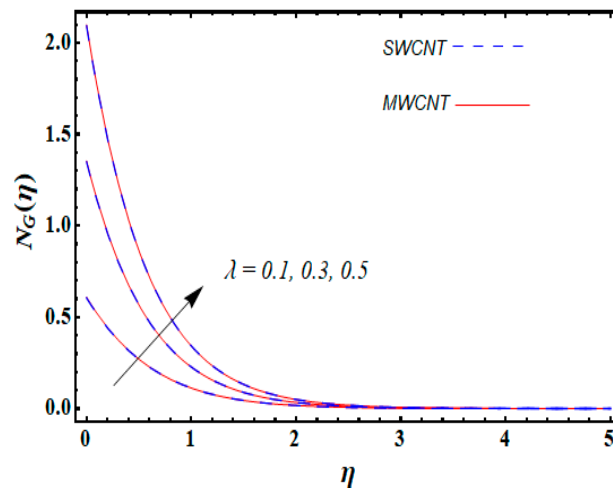


Figure 14. Consequence of  $\lambda$  on  $N_G(\eta)$ .

Table 4 shows that the skin friction coefficient is enhanced with increase in the values of the solid volume fraction of nanoparticles and suction parameter, while it declines for higher values of the porous medium, magnetic parameter, and bioconvection Rayleigh number. Table 5 demonstrates the numerical values of the Nusselt number for different varying parameters. It is found that the Nusselt number rises for larger estimates of solid volume fraction, radiation parameter, and Biot number, and decreases when the values of the magnetic parameter are increased. Table 6 displays the numerical value of the Sherwood number for varied parameters. The Sherwood number boosted with an increase in the values of the chemical reaction parameter and the Schmidt number, while it decreases with an increase in the values of the concentration stratification and buoyancy ratio parameter. Table 7 depicts the numerical value of motile density number versus different parameters. The motile density number increases for larger estimates of the Péclet number and microorganism concentration difference parameter and decreases for increasing values of the Rayleigh number.

**Table 4.** Numerical value of  $\frac{1}{(1-\phi)^{2.5}} f''(0)$ .

$\phi$	$k_1$	$V_0$	$R_b$	$M$	$\frac{1}{(1-\phi)^{2.5}} f''(0)$	
					SWCNTs	MWCNTs
0.1	0.5	1.0	0.1	1.0	1.11420	0.57810
0.2					1.23160	1.00280
0.3					1.47580	1.11930
	0.2				1.29720	1.26970
	0.3				1.22650	1.16470
	0.4				1.16610	1.07700
		0.5			1.04840	0.87042
		0.6			1.07060	0.89693
		0.7			1.09350	0.92345
			0.2		1.10830	0.94259
			0.3		1.05020	0.88198
			0.4		0.99171	0.82097
				0.5	1.46240	1.25400
				0.6	1.38720	1.19320
				0.7	1.32120	1.13840

**Table 5.** Numerical value of  $-\frac{k_{nf}}{k_f}(1 + R_d)\theta'(0)$ .

$\phi$	$R_d$	$B_1$	$M$	$-\frac{k_{nf}}{k_f}(1+R_d)\theta'(0)$	
				SWCNTs	MWCNTs
0.01	0.1	1.0	1.0	0.45621	0.45560
0.02				0.46268	0.46097
0.03				0.47205	0.46855
	0.2			0.47736	0.47659
	0.3			0.49760	0.49666
	0.4			0.51704	0.51594
		0.5		0.31751	0.31731
		0.7		0.38387	0.38351
		1.0		0.45621	0.45560
			1.0	0.45621	0.45560
			2.0	0.45279	0.45238
			3.0	0.45094	0.45063

**Table 6.** Numerical values of  $-g'(0)$ .

$S_c$	$C_r$	$n$	$N_r$	$-g'(0)$	
				SWCNTs	MWCNTs
0.1	0.1	0.1	0.5	0.31891	0.31882
0.5				0.50221	0.50155
0.9				0.74207	0.74087
	0.1			0.80642	0.80511
	0.2			0.88714	0.88613
	0.3			0.95695	0.95612
		0.2		0.73573	0.73379
		0.3		0.66795	0.66532
		0.4		0.60326	0.59988
			0.6	0.79903	0.79771
			0.7	0.79130	0.78997
			0.8	0.78319	0.78185

**Table 7.** Numerical values of  $Nn_x Ra_x^{-1/4}$ .

$L_b$	$Pe$	$R_b$	$\delta$	$-h'(0)$	
				SWCNTs	MWCNTs
0.5	0.5	0.1	0.1	0.83681	0.83535
0.6				0.91358	0.91207
0.7				0.99024	0.98870
	0.1			0.48494	0.48380
	0.2			0.57267	0.57146
	0.3			0.66056	0.65927
		0.2		0.82280	0.82132
		0.3		0.80759	0.80609
		0.4		0.79092	0.78938
			0.2	0.87679	0.87530
			0.3	0.91679	0.91528
			0.4	0.95681	0.95528

#### 4. Final Remarks

The flow of water based carbon nanotubes (SWCNT and MWCNT) fluid past a cone erected vertically is discussed numerically. The analysis is performed in the presence of motile organisms with solutal stratification in spongy media. Furthermore, the attributes of thermal radiation and chemical species are explored in the presence of entropy generation. The main outcomes of the analysis are:

- The velocity of the fluid diminishes with increasing values of the magnetic and suction parameters in the case of both nanotubes.
- The fluid's concentration is diminished for both SWCNT and MWCNT nanotubes versus higher values of solutal stratification.
- When increasing the temperature difference parameter, the entropy generation number decreases for both nanoparticles.
- The Sherwood number increases with increasing values of the chemical reaction parameter and the Schmidt number, while it decreases with increasing estimates of solutal stratification.
- The motile density number decreases with increasing values of the Péclet number.
- The skin friction coefficient increases for the suction parameter while decreasing for the bioconvection Rayleigh number.
- It is found that the Nusselt number increases with an increase in the estimates of solid volume fraction, radiation parameter, and Biot number, whereas it decreases with increasing values of the magnetic parameter.

**Author Contributions:** M.R. and M.M wrote the main manuscript text; M.M analysis and software; J.D.C modeled the problem; and F.H. prepared all figures and tables.

**Funding:** This work is supported by Zayed University, Abu Dhabi, UAE research fund.

**Conflicts of Interest:** Authors have no conflict of interest regarding this publication.

## Nomenclature

$u, v$	velocity components
$x, y$	coordinate
$K_r$	rate of chemical reaction
$K$	permeability parameter
$h_f$	convective parameter
$B_1$	Boit number
$N_r$	buoyancy ratio parameter
$V_0$	suction/injection parameter
$T, T_f$	temperature
$D_n$	diffusivity of microorganisms
$Pr$	Prandtl number
$C_p$	specific heat
$u_w$	stretching velocity along $x$ -direction
$B_0$	magnetic field of strength
$D_m$	Brownian diffusion coefficient
$C_f$	surface drag force
$Nu_x$	Nusselt number
$Pe$	bioconvection Péclet number
$C_r$	chemical reaction parameter
$Sc$	Schmidt number
$W_c$	maximum cell swimming speed
$k_1$	porous parameter
$R_b$	bioconvection Rayleigh number
$R_d$	radiation parameter
$Ra_x$	local Rayleigh number
$N_G$	entropy generation number
$L_b$	bioconvection Lewis number
$M$	magnetic parameter
<b>Greek Symbols</b>	
$\rho_{CNT}, \rho_f$	density
$\sigma^*$	Stephan-Boltzmann constant
$\mu_{nf}, \mu_f$	dynamic viscosity
$\tau_{xy}$	shear stress
$\alpha_{nf}$	modified thermal diffusivity
$(\rho C_p)_{nf}, (\rho C_p)_f$	heat capacity
$k_f, k_{nf}, k$	thermal conductivity
$\phi$	solid volume fraction of nanofluid
$\eta$	a scaled boundary-layer coordinate
$\Psi$	stream function
$q_w(x)$	the surface heat flux of nanoliquid film
$\beta$	thermal expansion coefficient
$f$	dimensionless stream function
$\theta$	dimensionless temperature
$\delta$	bioconvection constant
$\alpha$	temperature difference parameter
$\lambda$	diffusive constant parameter
$\zeta$	concentration difference

## References

1. Suleman, M.; Ramzan, M.; Zulfiqar, M.; Bilal, M.; Shafee, A.; Chung, J.D.; Lu, D.; Farooq, U. Entropy analysis of 3D non-Newtonian MHD nanofluid flow with nonlinear thermal radiation past over exponential stretched surface. *Entropy* **2018**, *20*, 930. [[CrossRef](#)]

2. Xiao, B.; Wang, W.; Zhang, X.; Long, G.; Chen, H.; Cai, H.; Deng, L. A novel fractal model for relative permeability of gas diffusion layer in proton exchange membrane fuel cell with capillary pressure effect. *Fractals* **2019**, *27*, 1950012. [[CrossRef](#)]
3. Xiao, B.; Wang, W.; Zhang, X.; Long, G.; Fan, J.; Chen, H.; Deng, L. A novel fractal solution for permeability and Kozeny–Carman constant of fibrous porous media made up of solid particles and porous fibers. *Powder Technol.* **2019**, *349*, 92–98. [[CrossRef](#)]
4. Long, G.; Liu, S.; Xu, G.; Wong, S.W.; Chen, H.; Xiao, B. A perforation-erosion model for hydraulic-fracturing applications. *SPE Prod. Oper.* **2018**, *33*, 770–783. [[CrossRef](#)]
5. Ramzan, M.; Chung, J.D.; Ullah, N. Radiative magnetohydrodynamic nanofluid flow due to gyrotactic microorganisms with chemical reaction and non-linear thermal radiation. *Int. J. Mech. Sci.* **2017**, *130*, 31–40. [[CrossRef](#)]
6. Lu, D.; Ramzan, M.; Ullah, N.; Chung, J.D.; Farooq, U. A numerical treatment of radiative nanofluid 3D flow containing gyrotactic microorganism with anisotropic slip, binary chemical reaction and activation energy. *Sci. Rep.* **2017**, *7*, 17008. [[CrossRef](#)] [[PubMed](#)]
7. Choi, S.U.; Eastman, J.A. Enhancing thermal conductivity of fluids with nanoparticles (No. ANL/MSD/CP-84938; CONF-951135-29). In Proceedings of the ASME International Mechanical Engineering Congress & Exposition, San Francisco, CA, USA, 12–17 November 1995.
8. Buongiorno, J. Convective transport in nanofluids. *J. Heat Transf.* **2006**, *128*, 240–250. [[CrossRef](#)]
9. Makinde, O.D.; Aziz, A. Boundary layer flow of a nanofluid past a stretching sheet with a convective boundary condition. *Int. J. Therm. Sci.* **2011**, *50*, 1326–1332. [[CrossRef](#)]
10. Ramzan, M.; Sheikholeslami, M.; Saeed, M.; Chung, J.D. On the convective heat and zero nanoparticle mass flux conditions in the flow of 3D MHD Couple Stress nanofluid over an exponentially stretched surface. *Sci. Rep.* **2019**, *9*, 562. [[CrossRef](#)]
11. Farooq, U.; Lu, D.; Ahmed, S.; Ramzan, M.; Chung, J.D.; Chandio, F.A. Computational analysis for mixed convective flows of viscous fluids with nanoparticles. *J. Therm. Sci. Eng. Appl.* **2019**, *11*, 021013. [[CrossRef](#)]
12. Reddy, Y.R.O.; Reddy, M.S.; Reddy, P.S. MHD boundary layer flow of SWCNT-water and MWCNT-water nanofluid over a vertical cone with heat generation/absorption. *Heat Transf. Asian Res.* **2019**, *48*, 539–555. [[CrossRef](#)]
13. Reddy, Y.; Reddy, M.S. Heat and Mass Transfer Analysis of Single Walled Carbon Nanotubes and Multi Walled Carbon Nanotubes-Water Nanofluid Flow Over Porous Inclined Plate with Heat Generation/Absorption. *J. Nanofluids* **2019**, *8*, 1147–1157. [[CrossRef](#)]
14. Sreedevi, P.; Reddy, P.S.; Chamkha, A.J. Magneto-hydrodynamics heat and mass transfer analysis of single and multi-wall carbon nanotubes over vertical cone with convective boundary condition. *Int. J. Mech. Sci.* **2018**, *135*, 646–655. [[CrossRef](#)]
15. Shehzad, N.; Zeeshan, A.; Ellahi, R.; Rashidi, S. Modelling study on internal energy loss due to entropy generation for non-darcy poiseuille flow of silver-water nanofluid: An application of purification. *Entropy* **2018**, *20*, 851. [[CrossRef](#)]
16. Zeeshan, A.; Shehzad, N.; Abbas, T.; Ellahi, R. Effects of Radiative Electro-Magnetohydrodynamics Diminishing Internal Energy of Pressure-Driven Flow of Titanium Dioxide-Water Nanofluid due to Entropy Generation. *Entropy* **2019**, *21*, 236. [[CrossRef](#)]
17. Suleman, M.; Ramzan, M.; Ahmad, S.; Lu, D.; Muhammad, T.; Chung, J.D. A Numerical Simulation of Silver–Water Nanofluid Flow with Impacts of Newtonian Heating and Homogeneous–Heterogeneous Reactions Past a Nonlinear Stretched Cylinder. *Symmetry* **2019**, *11*, 295. [[CrossRef](#)]
18. Sheikholeslami, M.; Shafee, A.; Ramzan, M.; Li, Z. Investigation of Lorentz forces and radiation impacts on nanofluid treatment in a porous semi annulus via Darcy law. *J. Mol. Liq.* **2018**, *272*, 8–14. [[CrossRef](#)]
19. Han, Z.; Fina, A. Thermal conductivity of carbon nanotubes and their polymer nanocomposites: A review. *Prog. Polym. Sci.* **2011**, *36*, 914–944. [[CrossRef](#)]
20. Shahzadi, I.; Sadaf, H.; Nadeem, S.; Saleem, A. Bio-mathematical analysis for the peristaltic flow of single wall carbon nanotubes under the impact of variable viscosity and wall properties. *Comput. Methods Programs Biomed.* **2017**, *139*, 137–147. [[CrossRef](#)]
21. Khan, M.I.; Rashid, M.; Hayat, T.; Khan, N.B.; Alsaedi, A. Physical aspects of Darcy-Forchheimer bidirectional flow in carbon nanotubes (SWCNTs and MWCNTs). *Int. J. Numer. Methods Heat Fluid Fl.* **2019**. [[CrossRef](#)]



22. Hayat, T.; Haider, F.; Muhammad, T.; Alsaedi, A. Numerical treatment for Darcy-Forchheimer flow of carbon nanotubes due to an exponentially stretching curved surface. *J. Cent. South Univ.* **2019**, *26*, 865–872. [[CrossRef](#)]
23. Iijima, S. Helical microtubules of graphitic carbon. *Nature* **1991**, *354*, 56. [[CrossRef](#)]
24. Bethune, D.S.; Kiang, C.H.; De Vries, M.S.; Gorman, G.; Savoy, R.; Vazquez, J.; Beyers, R. Cobalt-catalyzed growth of carbon nanotubes with single-atomic-layer walls. *Nature* **1993**, *363*, 605. [[CrossRef](#)]
25. Ramasubramaniam, R.; Chen, J.; Liu, H. Homogeneous carbon nanotube/polymer composites for electrical applications. *Appl. Phys. Lett.* **2003**, *83*, 2928–2930. [[CrossRef](#)]
26. Xue, Q.Z. Model for thermal conductivity of carbon nanotube-based composites. *Phys. B Condens. Matter* **2005**, *368*, 302–307. [[CrossRef](#)]
27. Muhammad, S.; Ali, G.; Shah, Z.; Islam, S.; Hussain, S. The rotating flow of magneto hydrodynamic carbon nanotubes over a stretching sheet with the impact of non-linear thermal radiation and heat generation/absorption. *Appl. Sci.* **2018**, *8*, 482. [[CrossRef](#)]
28. Kumar, R.; Kumar, R.; Sheikholeslami, M.; Chamkha, A.J. Irreversibility analysis of the three dimensional flow of carbon nanotubes due to nonlinear thermal radiation and quartic chemical reactions. *J. Mol. Liq.* **2019**, *274*, 379–392. [[CrossRef](#)]
29. Muhammad, T.; Lu, D.C.; Mahanthesh, B.; Eid, M.R.; Ramzan, M.; Dar, A. Significance of Darcy-Forchheimer porous medium in nanofluid through carbon nanotubes. *Commun. Theor. Phys.* **2018**, *70*, 361. [[CrossRef](#)]
30. Alshomrani, A.S.; Ullah, M.Z. Effects of Homogeneous–Heterogeneous Reactions and Convective Condition in Darcy–Forchheimer Flow of Carbon Nanotubes. *J. Heat Transf.* **2019**, *141*, 012405. [[CrossRef](#)]
31. Lu, D.; Li, Z.; Ramzan, M.; Shafee, A.; Chung, J.D. Unsteady squeezing carbon nanotubes based nano-liquid flow with Cattaneo–Christov heat flux and homogeneous–heterogeneous reactions. *Appl. Nanosci.* **2019**, *9*, 169–178. [[CrossRef](#)]
32. Ramzan, M.; Sheikholeslami, M.; Chung, J.D.; Shafee, A. Melting heat transfer and entropy optimization owing to carbon nanotubes suspended Casson nanoliquid flow past a swirling cylinder-A numerical treatment. *Aip Adv.* **2018**, *8*, 115130. [[CrossRef](#)]
33. Lu, D.; Ramzan, M.; Mohammad, M.; Howari, F.; Chung, J.D. A Thin Film Flow of Nanofluid Comprising Carbon Nanotubes Influenced by Cattaneo-Christov Heat Flux and Entropy Generation. *Coatings* **2019**, *9*, 296. [[CrossRef](#)]
34. Khan, W.A.; Khan, Z.H.; Rahi, M. Fluid flow and heat transfer of carbon nanotubes along a flat plate with Navier slip boundary. *Appl. Nanosci.* **2014**, *4*, 633–641. [[CrossRef](#)]
35. Abraham, A.; Dutta, P.; Mandal, J.K.; Bhattacharya, A.; Dutta, S. *Emerging Technologies in Data Mining and Information Security*; Springer: Singapore, 2018; Volume 2.



© 2019 by the authors. Licensee MDPI, Basel, Switzerland. This article is an open access article distributed under the terms and conditions of the Creative Commons Attribution (CC BY) license (<http://creativecommons.org/licenses/by/4.0/>).